A first-principles approach to finite temperature elastic constants

2010 J. Phys.: Condens. Matter 22 225404

(http://iopscience.iop.org/0953-8984/22/22/225404)

J. Phys.: Condens. Matter **22** (2010) 225404 (8pp) doi:10.1088/0953-8984/22/22/225404

A first-principles approach to finite temperature elastic constants

Y Wang, J J Wang, H Zhang, V R Manga, S L Shang, L-Q Chen and Z-K Liu

Department of Materials Science and Engineering, The Pennsylvania State University, University Park, PA 16802, USA

Received 22 March 2010, in final form 22 April 2010
Published 20 May 2010
Online at stacks.iop.org/JPhysCM/22/225404

Abstract

A first-principles approach to calculating the elastic stiffness coefficients at finite temperatures was proposed. It is based on the assumption that the temperature dependence of elastic stiffness coefficients mainly results from volume change as a function of temperature; it combines the first-principles calculations of elastic constants at 0 K and the first-principles phonon theory of thermal expansion. Its applications to elastic constants of Al, Cu, Ni, Mo, Ta, NiAl, and Ni_3Al from 0 K up to their respective melting points show excellent agreement between the predicted values and existing experimental measurements.

(Some figures in this article are in colour only in the electronic version)

1. Introduction

Recent developments in density functional theory (DFT) [1, 2] enable us to obtain reliable ground state properties of various materials. In particular, advances in computing resources and computational methods make it possible to perform routine first-principles calculations of elastic stiffness coefficients. There have been numerous reports of first-principles calculations of the elastic properties of solids by the total energy approach [3–5], stress–strain approach [6–12], and density functional perturbation theory [13–15]. However, almost all existing first-principles calculations of elastic constants were restricted to 0 K while the elastic stiffness coefficients of a material can decrease by over 20% as temperature increases [16–21]. The temperature dependence of the elastic stiffness coefficients of a material is important for predicting and understanding the mechanical strength, stability, and phase transitions of a material [22]. The main objective of this work is to propose a rather general and yet simple approach to determine the temperature effect of elastic stiffness coefficients. Our approach is based on the fact that the elastic moduli change is mainly controlled by volume [22–25], and it is the volume change with increasing temperature that results in the change of elastic moduli. We will discuss in detail the computational implementation and various physical subtleties and illustrate its applications to seven cubic metals as examples.

The rest of this paper is organized as follows. We will first summarize in section 2 the formulation in calculating the elastic stiffness coefficients and in section 3 the formulation in calculating the Helmholtz free energy. We will then introduce the quasistatic procedure of transforming the 0 K into finite temperature data in section 4. Section 5 shows how to convert the isothermal elastic stiffness coefficients to the isentropic elastic stiffness coefficients for cubic metals. Section 6 briefly explains details of first-principles computations using the VASP code. Section 7 presents our calculated temperature dependence of the isentropic elastic stiffness coefficients up to their respective melting points for fcc Al, fcc Cu, fcc Ni, bcc Mo, bcc Ta, cubic B2-NiAl, and cubic $L1_2$-Ni_3Al. Finally, section 8 is a short summary.

2. Elastic theory

According to the present status of the first-principles method [26, 27], the most convenient input data are the lattice vectors. Let us choose a reference state in which the lattice vectors are **a**, **b**, and **c** in Cartesian coordinates. For programming the calculation of elastic stiffness coefficients, it is more convenient to combine the three lattice vectors into a 3×3 matrix **R**:

$$\mathbf{R} = \begin{pmatrix} \mathbf{a} \\ \mathbf{b} \\ \mathbf{c} \end{pmatrix}. \tag{1}$$

The homogeneous deformation of a crystal with respect to the reference state **R** can then be expressed as:

$$\mathbf{R}' = \mathbf{RX}, \tag{2}$$

where the transformation matrix $\mathbf{X} = \mathbf{I} + \mathbf{D}$ with $\mathbf{I}$ being the unit 3×3 matrix and $\mathbf{D}$ being the 3×3 deformation matrix with elements d_{ij}, where $i, j = x, y$, and z are the axes of Cartesian coordinates.

By the definition of $\mathbf{D}$, there will be nine degrees of freedom to deform a crystal. We can demonstrate that three out of the nine are pure rotations which cannot result in energy change. The matrix $\mathbf{D}$ can be decomposed into the form:

$$\mathbf{D} = \mathbf{E} + \mathbf{U}, \tag{3}$$

where,

$$\mathbf{E} = \begin{pmatrix} e_1 & e_6/2 & e_5/2 \\ e_6/2 & e_2 & e_4/2 \\ e_5/2 & e_4/2 & e_3 \end{pmatrix}, \tag{4}$$

and

$$\mathbf{U} = \begin{pmatrix} 0 & u_6 & u_5 \\ -u_6 & 0 & u_4 \\ -u_5 & -u_4 & 0 \end{pmatrix}, \tag{5}$$

where $e_1 = d_{xx}$, $e_2 = d_{yy}$, $e_3 = d_{zz}$, $e_4 = d_{yz} + d_{zy}$, $e_5 = d_{xz} + d_{zx}$, $e_6 = d_{xy} + d_{yx}$, $u_4 = (d_{yz} - d_{zy})/2$, $u_5 = (d_{xz} - d_{zx})/2$, and $u_6 = (d_{xy} - d_{yx})/2$. Our discussion will be limited to small deformations. In such a case, $\mathbf{X}$ in equation (2) can then be rewritten as $\mathbf{X} = \mathbf{I} + \mathbf{E} + \mathbf{U} \cong (\mathbf{I} + \mathbf{E})(\mathbf{I} + \mathbf{U})$. Then, it is evident that $\mathbf{I} + \mathbf{U}$ is a pure rotation which will not result in energy change and can be neglected in deforming the lattice in the calculations of elastic stiffness coefficients.

We chose to use the elastic theory by Barron and Klein [28] based on the Helmholtz free energy from which one first derives the isothermal elastic stiffness coefficients. In the second-order approximation, the Helmholtz free energy change ΔF due to elastic deformation, with respect to the reference state $\mathbf{R}$ and temperature T, can be written as [29]:

$$\Delta F(T, \mathbf{R}') = V\left[\sum_{i=1}^{6} \sigma_i^0(T, \mathbf{R}) e_i + \tfrac{1}{2} \sum_{i,j=1}^{6} e_i c_{ij}^T(T, \mathbf{R}) e_j\right], \tag{6}$$

with the associated stress σ_i $(i = 1, 2, \ldots, 6)$ given in the form:

$$\sigma_i(T, \mathbf{R}') = \sigma_i^0(T, \mathbf{R}) + \sum_{j=1}^{6} c_{ij}^T(T, \mathbf{R}) e_j, \qquad (i = 1, 2, \ldots, 6) \tag{7}$$

where, $c_{ij}^T = c_{ji}^T$ is the isothermal elastic stiffness coefficient. In equations (6) and (7), σ_i^0 $(i = 1, 2, \ldots, 6)$ represent the stresses at the reference state $\mathbf{R}$ and temperature T before deformation.

3. Helmholtz free energy from the quasiharmonic approach

This section summarizes the necessary formula for programming purposes in calculating the thermodynamic quantities based on the quasiharmonic approach and thermal electronic excitations. For a system at the reference state $\mathbf{R}$ and temperature T, the Helmholtz free energy $F(\mathbf{R}, T)$ per atom can be approximated as [30–32]:

$$F(\mathbf{R}, T) = E_c(\mathbf{R}) + F_{\mathrm{ph}}(\mathbf{R}, T) + F_{\mathrm{el}}(\mathbf{R}, T), \tag{8}$$

where, in the framework of first-principles calculations, E_c is the 0 K static total energy; F_{ph} is the vibrational free energy of the lattice atoms given by [30]

$$F_{\mathrm{ph}}(\mathbf{R}, T) = k_{\mathrm{B}} T \frac{1}{N_{\mathbf{q}}} \sum_{\mathbf{q}}^{N_{\mathbf{q}}} \frac{1}{N} \sum_{j}^{3N} \ln\left\{2 \sinh\left[\frac{\hbar\omega_j(\mathbf{q})}{2k_{\mathrm{B}}T}\right]\right\}, \tag{9}$$

where k_{B} is the Boltzmann's constant, $N_{\mathbf{q}}$ is the number of sampled wavevector $\mathbf{q}$s, N is the number of atoms in the primitive unit cell, and $\hbar$ is the reduced Planck's constant. The last term F_{el} in equation (8) is the thermal electronic contribution to the free energy and an acceptable approximation to calculate F_{el} is to use the Mermin statistics [33–35] through

$$F_{\mathrm{el}}(\mathbf{R}, T) = E_{\mathrm{el}}(\mathbf{R}, T) - T S_{\mathrm{el}}(\mathbf{R}, T), \tag{10}$$

where the bare electronic entropy S_{el} takes the form:

$$S_{\mathrm{el}}(\mathbf{R}, T) = -k_{\mathrm{B}} \int n(\varepsilon, \mathbf{R})\{f(\varepsilon, T, \mathbf{R}) \ln f(\varepsilon, T, \mathbf{R}) + [1 - f(\varepsilon, T, \mathbf{R})] \ln[1 - f(\varepsilon, T, \mathbf{R})]\} \, \mathrm{d}\varepsilon, \tag{11}$$

where $n(\varepsilon, \mathbf{R})$ is the electronic density-of-states and f is the Fermi distribution:

$$f(\varepsilon, T, \mathbf{R}) = \frac{1}{\exp[\frac{\varepsilon - \mu(T, \mathbf{R})}{k_{\mathrm{B}}T}] + 1}. \tag{12}$$

We mention that $\mu(T, \mathbf{R})$ in equation (12) is the electronic chemical potential which is temperature dependent and should be carefully calculated to keep the number of electrons constant by solving the following equation:

$$\int n(\varepsilon, \mathbf{R}) f(\varepsilon, T, \mathbf{R}) \, \mathrm{d}\varepsilon = \int^{\varepsilon_{\mathrm{F}}} n(\varepsilon, \mathbf{R}) \, \mathrm{d}\varepsilon, \tag{13}$$

noting that ε_{F} is the Fermi energy at 0 K. With respect to equation (10), the thermal electronic energy E_{el}, due to the thermal electron excitations, can be calculated through

$$E_{\mathrm{el}}(T, \mathbf{R}) = \int n(\varepsilon, \mathbf{R}) f(\varepsilon, T, \mathbf{R}) \varepsilon \, \mathrm{d}\varepsilon - \int^{\varepsilon_{\mathrm{F}}} n(\varepsilon, \mathbf{R}) \varepsilon \, \mathrm{d}\varepsilon. \tag{14}$$

After the Helmholtz free energy is obtained as functions of T and $\mathbf{R}$, the equilibrium volume at the given temperature T and pressure P can be calculated by solving

$$-\left(\frac{\partial F(V(\mathbf{R}), T)}{\partial V}\right)_T = P. \tag{15}$$

Note that V is the atomic volume which is the determinant of the matrix $\mathbf{R}$ divided by the number of atoms in the cell determined by $\mathbf{R}$. Other thermodynamic functions can be obtained in the usual way from $F(\mathbf{R}, T)$; for example, entropy $S = -(\partial F/\partial T)_V$, internal energy $E = F + TS$, and the Gibbs free energy $G = F + PV$.

4. Quasistatic approximation

In principle, the general way to compute the finite temperature elastic stiffness coefficients is to calculate the second derivatives of the free energy F in equation (8) with respect to the lattice matrix $\mathbf{R}$ defined in equation (1). However, numerically this is not trivial work at the present since it involves calculation of the second derivatives of $F_{\rm ph}$. We learned in our previous works [6, 7, 10–12] that to get reliable second derivatives of E_c, both high energy cutoff and highly dense k-mesh setting (around $30 \times 30 \times 30$) were needed. For the static calculation which just uses the primitive unit cell, this is not a problem. However, for the calculation of the phonon density-of-states (PDOS) which uses supercells (the supercells contain over 30 atoms in the present work) for both reference state and the deformed state, this is a tremendous cost of computational resources. We alternatively neglect the contributions of $F_{\rm ph}$, and for simplicity of calculation we also neglect the contributions of $F_{\rm el}$ to these second derivatives (we assume the contributions of $F_{\rm el}$ are small), retaining only E_c. The procedure can therefore be named as a quasistatic approximation, in analogy to the quasiharmonic approximation [36] to thermodynamics in phonon theory, where the temperature dependences of the various thermodynamic quantities are extracted from the volume-dependences of the PDOS calculated at 0 K. A similar procedure was employed by Kadas *et al* [37], though they calculated thermal expansion using the Debye model. We also apply a similar quasistatic approximation in calculating the thermal expansion, which is detailed below.

4.1. Quasistatic approximation for thermal expansion

For materials with symmetry lower than cubic, thermal expansion is in general anisotropic. Our quasistatic approximation to the thermal expansion is to just consider the 0 K dependence of $\mathbf{R}$ in equation (1) on V with respect to which $\mathbf{R}$ is optimized at 0 K. To implement this approximation, we first define

$$\mathbf{\Lambda} = \mathbf{R}^{-1}\left(\frac{\partial \mathbf{R}}{\partial V}\right)_{T=0}\frac{\partial V}{\partial T}, \tag{16}$$

where $\mathbf{R}^{-1}$ represents the inverse matrix of $\mathbf{R}$. Then the thermal expansion coefficient tensor α_j ($j = 1, 2, \ldots, 6$) can be calculated through $\alpha_1 = \Lambda_{11}$, $\alpha_2 = \Lambda_{22}$, $\alpha_3 = \Lambda_{33}$, $\alpha_4 = \Lambda_{23} + \Lambda_{32}$, $\alpha_5 = \Lambda_{13} + \Lambda_{31}$, and $\alpha_6 = \Lambda_{12} + \Lambda_{21}$. The quasistatic approximation has correctly predicted the thermal expansion of MgB_2 [38, 39] of which the linear thermal expansion coefficient in the c direction is almost double that in the a direction [40].

4.2. Quasistatic approximation for elastic stiffness coefficients

We calculate the temperature dependences of elastic stiffness coefficients by application of a systematic three-step procedure. The first step in this procedure is calculating the static elastic stiffness coefficients at 0 K as a function of volume using a stress–strain approach [6–12]. In the second step, the equilibrium volume $V(T, P)$ at the given T and P is calculated using the first-principles quasiharmonic approach [41–43]. In the third step, the calculated elastic stiffness coefficients from the first step at the volume $V(T, P)$ are approximated as those at finite temperatures.

In the above procedure, it is assumed that the temperature dependences of elastic stiffness coefficients are solely caused by thermal expansion. There is ample experimental evidence that lends support to the approximation, e.g. observations of the temperature dependence of isothermal bulk modulus [24], isentropic bulk modulus and shear modulus [23], and the Elinvar effect [25]. From the data for 16 cubic solids, Swenson [24] observed that the isothermal bulk modulus was almost solely a function of volume. By inspecting through 14 solids of significance to geophysics at high temperatures, Anderson and Isaak [23] found that it was a reasonable practice to treat both the isentropic bulk modulus and shear modulus only as a function of volume. For Elinvar [25], it was found that its elasticity was constant over a wide range of temperatures due to the lack of thermal expansion. The procedure is also supported by the theoretical calculation for Ta within the particle-in-a-cell model by Gülseren and Cohen [22] who found that the elastic stiffness coefficients depend primarily on volume, while the thermal effects at constant volume are quite small.

5. Conversion between isothermal and isentropic conditions

It should be mentioned that most of the experimental data [16–19, 21, 44–51] of elastic stiffness coefficients are usually reported as isentropic elastic stiffness coefficients, therefore the calculated isothermal elastic stiffness coefficients must be converted in order to be compared with experiments. According to the approximation by Davies [52], the isothermal elastic stiffness coefficients, c_{ij}^S, are related to the isentropic elastic stiffness coefficients by

$$c_{ij}^S(T, \mathbf{R}) = c_{ij}^T(T, \mathbf{R}) + \frac{TV\lambda_i\lambda_j}{C_V}, \tag{17}$$

where the isochoric heat capacity is calculated as $C_V = (\partial E/\partial T)_V$ and

$$\lambda_i = -\sum_j \alpha_j c_{ij}^T(T, \mathbf{R}). \tag{18}$$

With the help of equations (16) and (18), equation (17) can be applied to all materials with any space group symmetries. For cubic materials, equation (17) can be simplified as [22]:

$$c_{44}^S = c_{44}^T, \tag{19}$$

$$c_{11}^S = c_{11}^T + \Delta, \tag{20}$$

$$c_{12}^S = c_{12}^T + \Delta, \tag{21}$$

where [53]

$$\Delta = TV(\beta B_T)^2/C_V, \tag{22}$$

where $B_T = V(\partial^2 F/\partial V^2)_T$ is the isothermal bulk modulus and $\beta = (\partial V/\partial T)_P/V$ is the volume thermal expansion coefficient. Note that the isothermal c_{44}^T and isentropic c_{44}^S are equal.

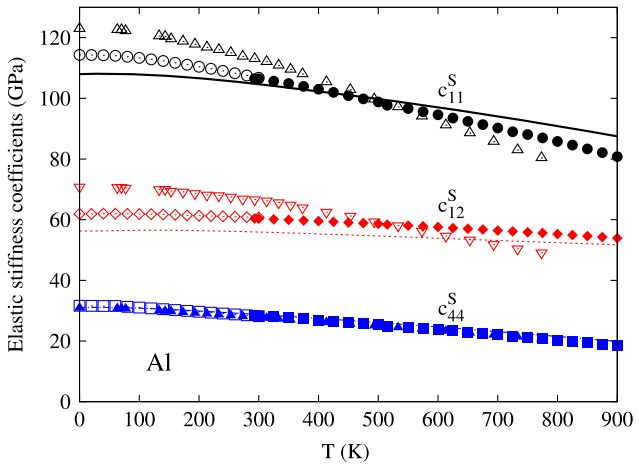

Figure 1. Calculated isentropic elastic stiffness coefficients (c_{11}^S: black solid line, c_{12}^S: red dashed line, and c_{44}^S: blue dot–dashed solid line (overlapped with experimental points)) of Al in comparison with experimental data of Kamm *et al* [18] (c_{11}^S: ○, c_{12}^S: ◇, and c_{44}^S: □), Gerlich and Fisher [17] (c_{11}^S: ●, c_{12}^S: ◆, and c_{44}^S: ■), and those from Sutton [19] (c_{11}^S: △, c_{12}^S: ▽, and c_{44}^S: ▲).

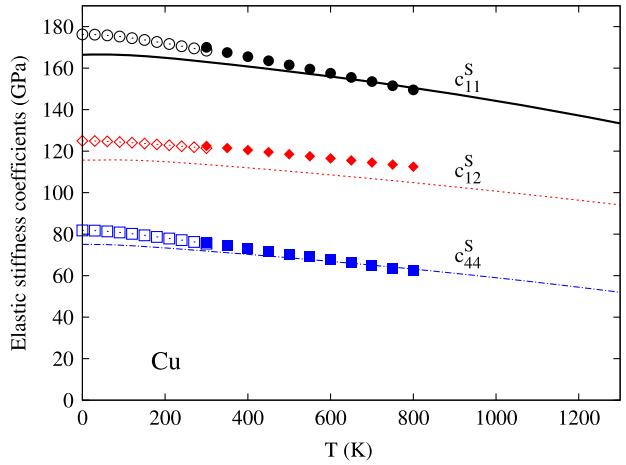

Figure 2. Calculated isentropic elastic stiffness coefficients (c_{11}^S: black solid line, c_{12}^S: red dashed line, and c_{44}^S: blue dot–dashed solid line) of Cu in comparison with experimental data of Overton *et al* [48] (c_{11}^S: ○, c_{12}^S: ◇, and c_{44}^S: □) and Chang and Himmel [45] (c_{11}^S: ●, c_{12}^S: ◆, and c_{44}^S: ■).

6. Computational details

The prototypes of the present work are cubic metal Al, Cu, Ni, Mo, Ta, NiAl, and Ni_3Al at zero pressure which means that the reference **R** in equation (6) is determined by setting $P = 0$ in equation (15). The procedure in calculating the 0 K elastic stiffness coefficients as a function of **R** follows the previous works [9, 11, 12]. To calculate E_c in equation (8), we have employed the projector-augmented wave (PAW) method [26, 27] within the generalized gradient approximation (GGA) of Perdew–Burke–Ernzerhof (PBE) [2] implemented in the VASP package [26, 27].

To calculate the phonon frequencies in equation (9), we have employed the ATAT code [54] which serves as the interface to the first-principles code, typically VASP.

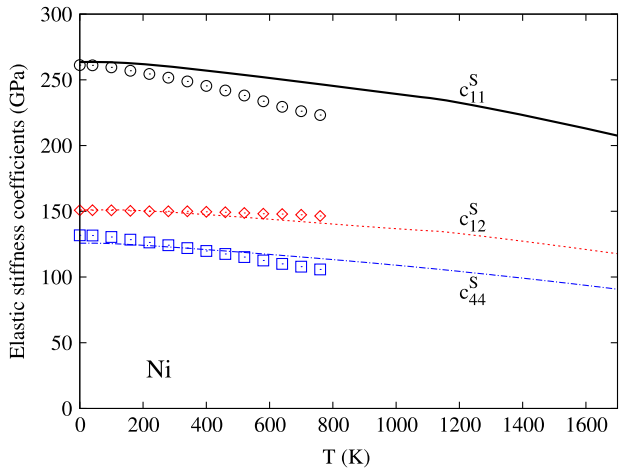

Figure 3. Calculated isentropic elastic stiffness coefficients (c_{11}^S: black solid line, c_{12}^S: red dashed line, and c_{44}^S: blue dot–dashed solid line) of Ni in comparison with experimental data of Alers *et al* [44] (c_{11}^S: ○, c_{12}^S: ◇, and c_{44}^S: □).

To consider the thermal expansion, we first calculate the frequencies at five volumes (with respect to each of which **R** is optimized at 0 K with the volume fixed) starting from the 0 K equilibrium volume with volume increment of 6%. At any given T, we calculate the Helmholtz free energy at the five volumes. We then employ the cubic spline interpolation to find the minima of $F(\mathbf{R}, T)$ as a function of **R** which means that we do not use any equation-of-states fitting in this work. We find that this approach is efficient, stable, and accurate as can be seen in the results given in the following sections.

7. Results

The calculated temperature dependences of the isentropic elastic stiffness coefficients of Al, Cu, Ni, Mo, Ta, NiAl, and Ni_3Al are plotted in figures 1–7, respectively, together with the available experimental data from our best knowledge for Al [17–19], Cu [45, 48], Ni [44], Mo [16, 47], Ta [16, 21], NiAl [46, 50], and Ni_3Al [49, 51]. In these figures, the calculated c_{11}^S, c_{12}^S, and c_{44}^S have been plotted as solid (black), dotted (red), and dot–dashed (blue) lines, respectively. The measured c_{11}^S, c_{12}^S, and c_{44}^S are plotted using black, red, and blue points, respectively.

The experimental data for Al in figure 1 are from [18, 17, 19]. While no deviations are seen between the ultrasonic measurements [18, 17] and the magnetoacoustic measurement [19] for c_{44}^S, it is seen that there exist quite large deviations between the ultrasonic measurements [18, 17] and the magnetoacoustic measurement [19] for c_{11}^S and c_{12}^S. The present calculation is in better agreement with the ultrasonic measurements than the magnetoacoustic measurement.

For the other six metals, the experimental data of Overton *et al* [48] and Chang and Himmel [45] for Cu in figure 2 are all from ultrasonic measurements; the experimental data of Alers *et al* [44] for Ni in figure 3 are from ultrasonic measurement under an applied magnetic field of 10 kOe to minimize the effects of magnetic phase transition; the experimental data

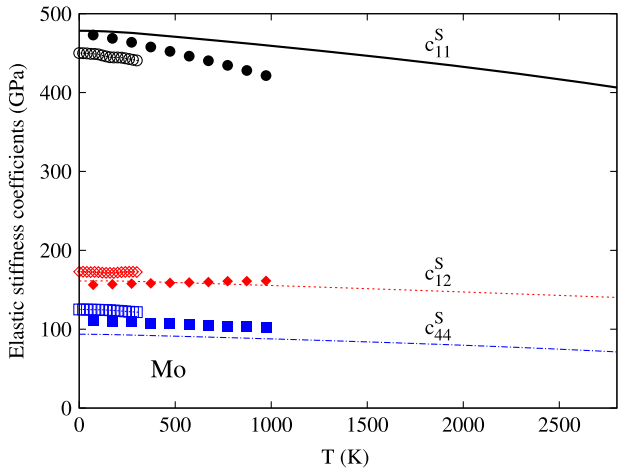

Figure 4. Calculated isentropic elastic stiffness coefficients (c_{11}^S: black solid line, c_{12}^S: red dashed line, and c_{44}^S: blue dot–dashed solid line) of Mo in comparison with experimental data of Featherston and Neighbors [16] (c_{11}^S: ○, c_{12}^S: ◇, and c_{44}^S: □) and Dickinson and Armstrong [47] (c_{11}^S: ●, c_{12}^S: ◆, and c_{44}^S: ■).

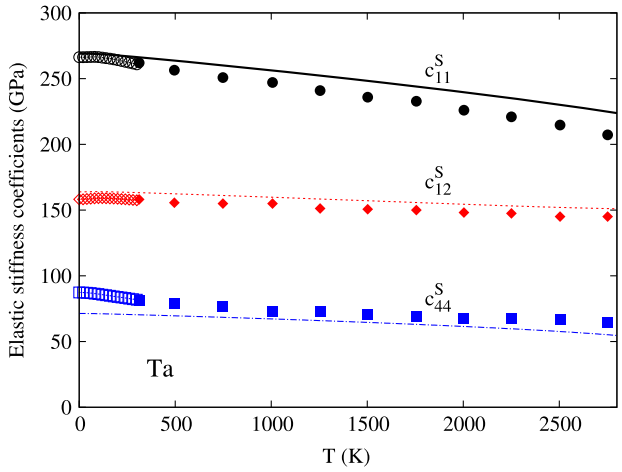

Figure 5. Calculated isentropic elastic stiffness coefficients (c_{11}^S: black solid line, c_{12}^S: red dashed line, and c_{44}^S: blue dot–dashed solid line) of Ta in comparison with experimental data of Featherston and Neighbors [16] (c_{11}^S: ○, c_{12}^S: ◇, and c_{44}^S: □) and Walker and Bujard [21] (c_{11}^S: ●, c_{12}^S: ◆, and c_{44}^S: ■).

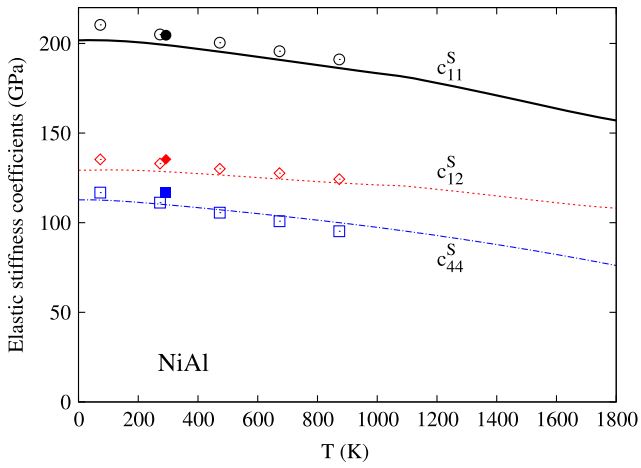

Figure 6. Calculated isentropic elastic stiffness coefficients (c_{11}^S: black solid line, c_{12}^S: red dashed line, and c_{44}^S: blue dot–dashed solid line) of NiAl in comparison with experimental data of Rusović and Warlimont [50] (c_{11}^S: ○, c_{12}^S: ◇, and c_{44}^S: □) and Davenport *et al* [46] (c_{11}^S: ●, c_{12}^S: ◆, and c_{44}^S: ■).

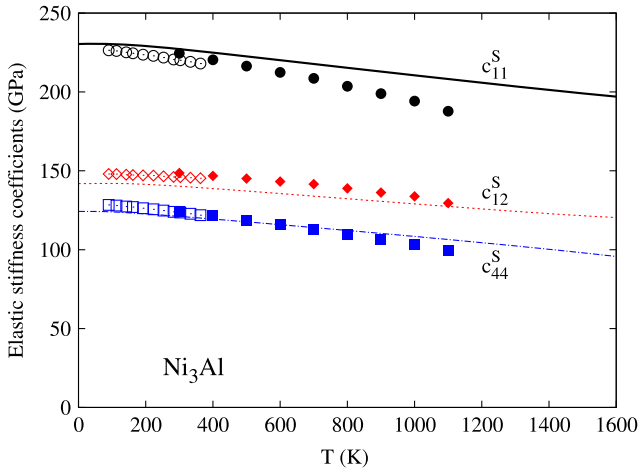

Figure 7. Calculated isentropic elastic stiffness coefficients (c_{11}^S: black solid line, c_{12}^S: red dashed line, and c_{44}^S: blue dot–dashed solid line) of Ni_3Al in comparison with experimental data of Tanaka and Koiwa [51] (c_{11}^S: ○, c_{12}^S: ◇, and c_{44}^S: □) and Prikhodko *et al* [49] (c_{11}^S: ●, c_{12}^S: ◆, and c_{44}^S: ■).

for Mo in figure 4 are from ultrasonic measurement by Featherston and Neighbors [16] and the thin-rod resonance technique by Dickinson and Armstrong [47]; the experimental data for Ta in figure 5 are from ultrasonic measurements by Featherston and Neighbors [16] and by Walker and Bujard [21]; the experimental data for NiAl in figure 6 are from ultrasonic measurements by Rusović and Warlimont [50] and by Davenport *et al* [46]; and the experimental data for Ni_3Al in figure 7 are from rectangular parallelepiped resonance measurements by Tanaka and Koiwa [51] and by Prikhodko *et al* [49].

Comparing the calculated values of c_{11}^S, c_{12}^S, and c_{44}^S for the seven metals with experiments we get a useful test of the accuracy of the method and the precision of our calculations. The overall observation is that all the calculated values of c_{11}^S, c_{12}^S, and c_{44}^S decrease with increasing temperature and approach linearity at higher temperatures and zero slope at zero temperature, being in agreement with experiments. For c_{12}^S and c_{44}^S, excellent agreements with experiments for the decreasing rates with temperature increase have been obtained by the present theoretical calculations. For c_{11}^S, the calculated decreasing rates with increasing temperature are (except NiAl) slightly smaller than the corresponding experimental results. The discrepancies found in the c_{11}^Ss could be attributed to the neglecting of the contributions of $F_{\rm ph}$ and $F_{\rm el}$ to these second derivatives. Accordingly, in figures 8–14 we compare the calculated bulk moduli without invoking the quasistatic approximation with those calculated with invoking the quasistatic approximation. In fact, the isentropic bulk modulus can be calculated from equation (8)

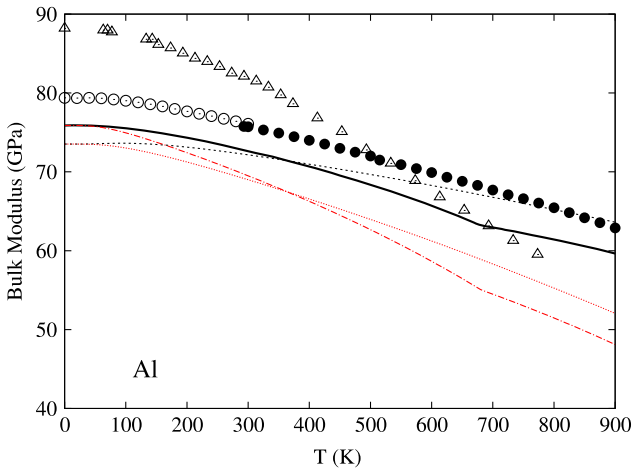

Figure 8. Calculated isentropic bulk moduli without the quasistatic approximation (black solid line) and with the quasistatic approximation (black dash line) as well as the calculated isothermal bulk moduli without the quasistatic approximation (red dot–dashed line) and with the quasistatic approximation (red dotted line) for Al. The experimental data (calculated on the measured c_{11}^S and c_{12}^S using equation (26)) are from Kamm *et al* [18] (○), Gerlich and Fisher [17] (●), and Sutton [19] (△).

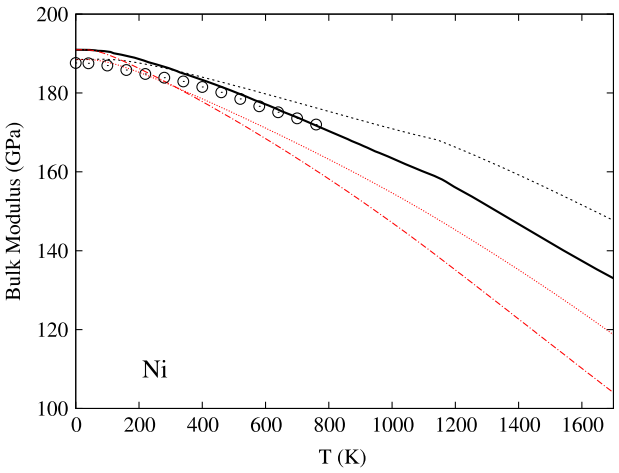

Figure 10. Calculated isentropic bulk moduli without the quasistatic approximation (black solid line) and with the quasistatic approximation (black dash line) as well as calculated isothermal bulk moduli without the quasistatic approximation (red dot–dashed line) and with the quasistatic approximation (red dotted line) for Ni. The experimental data (calculated on the measured c_{11}^S and c_{12}^S using equation (26)) are from Alers *et al* [44] (○).

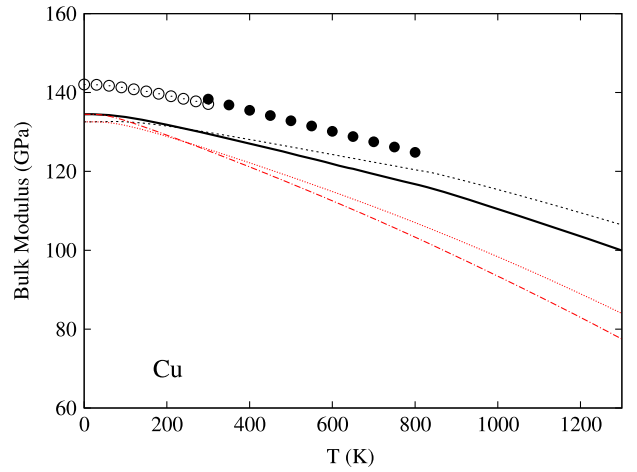

Figure 9. Calculated isentropic bulk moduli without the quasistatic approximation (black solid line) and with the quasistatic approximation (black dash line) as well as calculated isothermal bulk moduli without the quasistatic approximation (red dot–dashed line) and with the quasistatic approximation (red dotted line) for Cu. The experimental data (calculated on the measured c_{11}^S and c_{12}^S using equation (26)) are from Overton *et al* [48] (○) and Chang and Himmel [45] (●).

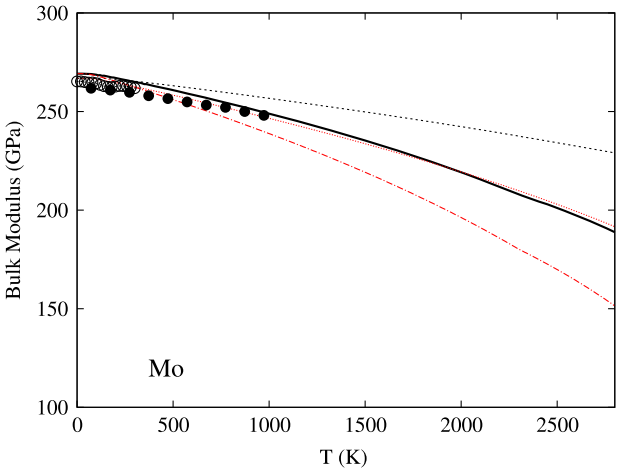

Figure 11. Calculated isentropic bulk moduli without the quasistatic approximation (black solid line) and with the quasistatic approximation (black dash line) as well as calculated isothermal bulk moduli without the quasistatic approximation (red dot–dashed line) and with the quasistatic approximation (red dotted line) for Mo. The experimental data (calculated on the measured c_{11}^S and c_{12}^S using equation (26)) are from Featherston and Neighbors [16] (○) and Dickinson and Armstrong [47] (●).

where the contributions of $F_{\rm ph}$ and $F_{\rm el}$ are considered:

$$B_S = B_T C_P / C_V = B_T + \Delta, \tag{23}$$

where C_P is the isobaric heat capacity which can be calculated as [55]

$$C_P = C_V + VTB_T\beta^2. \tag{24}$$

In comparison, from the quasistatic c_{11} and c_{12}, the bulk modulus can be calculated as [22]

$$B_T = \frac{C_{11}^T + 2C_{12}^T}{3} \tag{25}$$

and

$$B_S = \frac{C_{11}^S + 2C_{12}^S}{3}. \tag{26}$$

The small kink shown in some of the curves of figures 8–14 at high temperature is due to the numerical errors in calculating the second derivatives using the cubic spline method. In general, in the sense of the overall agreement with the experiments, the calculated results within the present quasistatic approximation are quite similar to those calculated without invoking the quasistatic approximation.

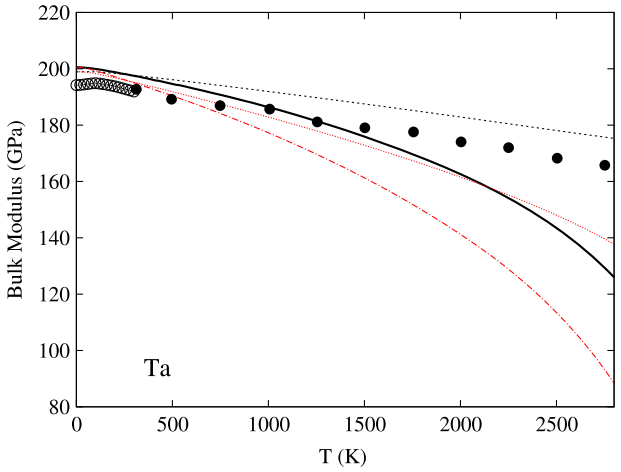

Figure 12. Calculated isentropic bulk moduli without the quasistatic approximation (black solid line) and with the quasistatic approximation (black dash line) as well as calculated isothermal bulk moduli without the quasistatic approximation (red dot–dashed line) and with the quasistatic approximation (red dotted line) for Ta. The experimental data (calculated on the measured c_{11}^S and c_{12}^S using equation (26)) are from Featherston and Neighbors [16] (○) and Walker and Bujard [21] (●).

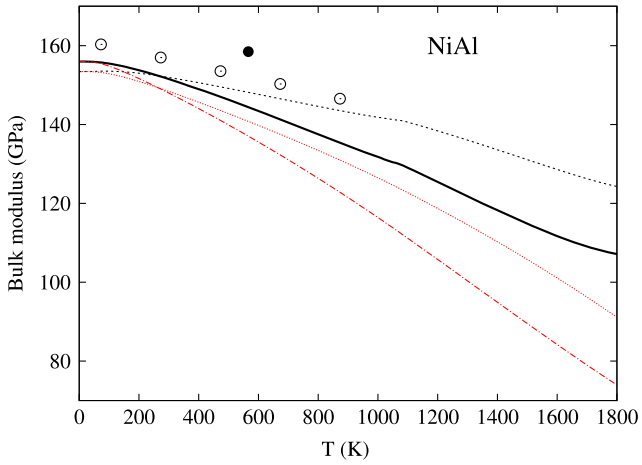

Figure 13. Calculated isentropic bulk moduli without the quasistatic approximation (black solid line) and with the quasistatic approximation (black dash line) as well as calculated isothermal bulk moduli without the quasistatic approximation (red dot–dashed line) and with the quasistatic approximation (red dotted line) for NiAl. The experimental data (calculated on the measured c_{11}^S and c_{12}^S using equation (26)) are from Rusović and Warlimont [50] (○) and Davenport *et al* [46] (●).

8. Conclusion and outlook

Based on the practical knowledge for a material that the main effect of temperature for the elasticity is due to thermal expansion, we have presented a first-principles procedure to calculate the temperature dependences of elastic stiffness coefficients by combining the quasistatic approximation to elasticity and the quasiharmonic phonon approximation to volume expansion. As prototypes, the elastic stiffness coefficients of seven cubic metals, Al, Cu, Ni, Mo, Ta, NiAl, and Ni_3Al at zero pressure, have been investigated for temperature ranges from 0 K up to their respective melting points. Being in agreement with experimental data, the calculations show that all the three elastic stiffness coefficients decrease with temperature increase for the seven metals. For c_{12}^S and c_{44}^S, the calculated temperature dependences are in excellent agreement with available ultrasonic experimental data, while for c_{11}^S, the calculated decreasing rates with temperature increase are slightly smaller than in experiments.

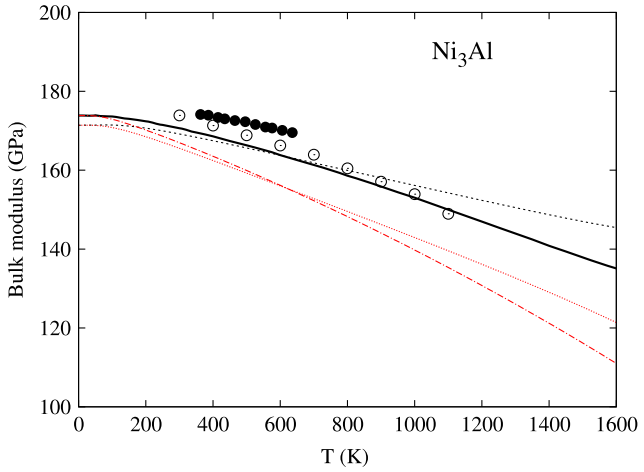

Figure 14. Calculated isentropic bulk moduli without the quasistatic approximation (black solid line) and with the quasistatic approximation (black dash line) as well as calculated isothermal bulk moduli without the quasistatic approximation (red dot–dashed line) and with the quasistatic approximation (red dotted line) for Ni_3Al. The experimental data (calculated on the measured c_{11}^S and c_{12}^S using equation (26)) are from Tanaka and Koiwa [51] (○) and Prikhodko *et al* [49] (●).

Acknowledgments

This work is funded by the Office of Naval Research (ONR) under contract No. N0014-07-1-0638 and the National Science Foundation (NSF) through grant No. DMR-0510180. First-principles calculations were carried out on the LION clusters at the Pennsylvania State University supported by the Materials Simulation Center and the Research Computing and Cyberinfrastructure unit at the Pennsylvania State University. High performance computing resources at the ARSC Allocated Distributed Center of the Department of Defense High Performance Computing Modernization Program through the Army Contract No. W911QX-07-P-0291 and at the National Energy Research Scientific Computing Center supported by the Office of Science of the US Department of Energy under DE-AC02-05CH11231 were also used in the present calculations.

References

[1] Kohn W and Sham L J 1965 *Phys. Rev.* **140** 1133
[2] Perdew J P, Burke K and Ernzerhof M 1996 *Phys. Rev. Lett.* **77** 3865
[3] Bercegeay C and Bernard S 2005 *Phys. Rev.* B **72** 214101
[4] Gressmann T, Wohlschlogel M, Shang S, Welzel U, Leineweber A, Mittemeijer E J and Liu Z K 2007 *Acta Mater.* **55** 5833

[5] Le Page Y and Saxe P 2001 *Phys. Rev.* B **63** 174103
[6] Ganeshan S, Shang S L, Wang Y and Liu Z K 2009 *Acta Mater.* **57** 3876
[7] Ganeshan S, Shang S L, Zhang H, Wang Y, Mantina M and Liu Z K 2009 *Intermetallics* **17** 313
[8] Kim D E, Shang S L and Liu Z K 2009 *Comput. Mater. Sci.* **47** 254
[9] Le Page Y and Saxe P 2002 *Phys. Rev.* B **65** 104104
[10] Shang S L, Sheng G, Wang Y, Chen L Q and Liu Z K 2009 *Phys. Rev.* B **80** 052102
[11] Shang S L, Wang Y and Liu Z K 2007 *Appl. Phys. Lett.* **90** 101909
[12] Zhang J X, Li Y L, Wang Y, Liu Z K, Chen L Q, Chu Y H, Zavaliche F and Ramesh R 2007 *J. Appl. Phys.* **101** 114105
[13] Baroni S, Giannozzi P and Testa A 1987 *Phys. Rev. Lett.* **59** 2662
[14] Hamann D R, Wu X F, Rabe K M and Vanderbilt D 2005 *Phys. Rev.* B **71** 035117
[15] Wu X, Vanderbilt D and Hamann D R 2005 *Phys. Rev.* B **72** 035105
[16] Featherston F H and Neighbours J R 1963 *Phys. Rev.* **130** 1324
[17] Gerlich D and Fisher E S 1969 *J. Phys. Chem. Solids* **30** 1197
[18] Kamm G N and Alers G A 1964 *J. Appl. Phys.* **35** 327
[19] Sutton P M 1953 *Phys. Rev.* **91** 816
[20] Vaks V G, Zarochentsev E V, Kravchuk S P and Safronov V P 1978 *J. Phys. F: Met. Phys.* **8** 725
[21] Walker E and Bujard P 1980 *Solid State Commun.* **34** 691
[22] Gülseren O and Cohen R E 2002 *Phys. Rev.* B **65** 064103
[23] Anderson O L and Isaak D G 1995 *Mineral Physics and Crystallography: A Handbook of Physical Constants* ed T J Ahrens, (Washington, DC: The American Geophysical Union) p 64
[24] Swenson C A 1968 *J. Phys. Chem. Solids* **29** 1337
[25] Wasserman E F 1990 *Ferromagnetic Materials* ed K H J Bushow and E P Wohlfarth (Amsterdam: Elsevier Science) p 238
[26] Blöchl P E 1994 *Phys. Rev.* B **50** 17953
[27] Kresse G and Joubert D 1999 *Phys. Rev.* B **59** 1758
[28] Barron T H K and Klein M L 1965 *Proc. Phys. Soc.* **85** 523
[29] Alouani M, Albers R C and Methfessel M 1991 *Phys. Rev.* B **43** 6500
[30] Wallace D C 1972 *Thermodynamics of Crystalls* (New York: Wiley)
[31] Wang Y, Liu Z K and Chen L Q 2004 *Acta Mater.* **52** 2665
[32] Wang Y, Liu Z K, Chen L Q, Burakovsky L and Ahuja R 2006 *J. Appl. Phys.* **100** 023533
[33] Landau L D and Lifshitz E M 1980–1981 *Statistical Physics* (Oxford: Pergamon)
[34] Wang Y 2000 *Phys. Rev.* B **61** 11863
[35] Wang Y, Chen D Q and Zhang X W 2000 *Phys. Rev. Lett.* **84** 3220
[36] Baroni S, de Gironcoli S, Dal Corso A and Giannozzi P 2001 *Rev. Mod. Phys.* **73** 515
[37] Kadas K, Vitos L, Ahuja R, Johansson B and Kollar J 2007 *Phys. Rev.* B **76** 235109
[38] Saengdeejing A, Saal J E, Wang Y and Liu Z K 2007 *Appl. Phys. Lett.* **90** 151920
[39] Saengdeejing A, Wang Y and Liu Z K 2010 *Intermetallics* **18** 803
[40] Birkedal H, Van Beek W, Emerich H and Pattison P 2003 *J. Mater. Sci. Lett.* **22** 1069
[41] Arroyave R, Shin D and Liu Z K 2005 *Acta Mater.* **53** 1809
[42] Shang S L, Wang Y, Arroyave R and Liu Z K 2007 *Phys. Rev.* B **75** 092101
[43] Wang Y, Hector L G, Zhang H, Shang S L, Chen L Q and Liu Z K 2008 *Phys. Rev.* B **78** 104113
[44] Alers G A, Neighbours J R and Sato H 1960 *J. Phys. Chem. Solids* **13** 40
[45] Chang Y A and Himmel L 1966 *J. Appl. Phys.* **37** 3567
[46] Davenport T, Zhou L and Trivisonno J 1999 *Phys. Rev.* B **59** 3421
[47] Dickinson J M and Armstrong P E 1967 *J. Appl. Phys.* **38** 602
[48] Overton W C and Gaffney J 1955 *Phys. Rev.* **98** 969
[49] Prikhodko S V, Carnes J D, Isaak D G, Yang H and Ardell A J 1999 *Metall. Mater. Trans.* A **30** 2403
[50] Rusović N and Warlimont H 1977 *Phys. Status Solidi* a **44** 609
[51] Tanaka K and Koiwa M 1996 *Intermetallics* **4** S29
[52] Davies G F 1974 *J. Phys. Chem. Solids* **35** 1513
[53] Orlikowski D, Söderlind P and Moriarty J A 2006 *Phys. Rev.* B **74** 054109
[54] van de Walle A, Asta M and Ceder G 2002 *CALPHAD* **26** 539
[55] Wang Y and Li L 2000 *Phys. Rev.* B **62** 196